

The non-Boussinesq lock-exchange problem. Part 1. Theory and experiments

By RYAN J. LOWE†, JAMES W. ROTTMAN
AND P. F. LINDEN

Department of Mechanical and Aerospace Engineering, University of California, San Diego, 9500
Gilman Drive, La Jolla, CA 92093-0411, USA

(Received 26 March 2004 and in revised form 17 January 2005)

The results of an experimental study of the non-Boussinesq lock-exchange problem are described. The experiments were performed in a rectangular channel using water and either a sodium iodide solution or a sodium chloride solution as the two fluids. These combinations of fluids have density ratios (light over heavy density) in the range 0.61 to 1. A two-layer hydraulic theory is developed to model the experiments. The theory assumes that a light gravity current propagates in one direction along the top of the channel and a heavy gravity current propagates in the opposite direction along the bottom of the channel. The two currents are assumed to be connected by either a combination of an internal bore and an expansion wave, or just an expansion wave. The present results, previous experimental results and two-dimensional numerical simulations from a companion paper are compared with the theory. The results of the comparison lead to the conclusion that the theory without the internal bore is the most appropriate.

1. Introduction

The so-called lock-exchange experiment is simple in concept. In a closed horizontal channel insert a vertical barrier. On one side of this barrier fill the channel with fluid and on the other side fill the channel with another fluid of different density. Then remove the barrier and watch the resulting flow. Despite the simplicity of execution of this experiment it results in a wide variety of flow phenomena, some of which still defy definitive theoretical explanation, that serve as prototypes for a variety of geophysical and industrial flows. In simplest terms the removal of the barrier results in a gravity current of the lighter fluid propagating at constant speed along the upper surface of the channel into the heavy fluid and in the opposite direction a gravity current of the heavier fluid propagating also at constant speed along the bottom of the channel.

A large number of laboratory experiments have been performed for this type of flow. Most of these experiments were for fluids with only slightly different densities – the Boussinesq case – which is representative of most geophysical flows. Among these experiments are those reported by Keulegan (1958), Barr (1967), Simpson & Britter (1979), Rottman & Simpson (1983), Huppert & Simpson (1980) and Shin, Dalziel & Linden (2004). The lock exchange problem for Boussinesq fluids has been simulated

† Present address: Department of Civil and Environmental Engineering, M42 Terman Engineering Center, Stanford University, Stanford, CA, 94305-4020, USA.

numerically by Daly & Pracht (1968), Klemp, Rotunno & Skamarock (1994) and Härtel, Meiburg & Necker (2000).

In this paper we are concerned with lock exchange involving fluids with large density differences – the non-Boussinesq case. Non-Boussinesq gravity currents are important in releases of dense gases into the atmosphere. These gases are often stored as liquids at low temperatures and on release have densities more than twice that of the ambient air. Fires in semi-enclosed spaces, such as a tunnel or a room, produce gravity currents when the hot combustion products reach the ceiling and then flow horizontally. Temperatures can easily reach 1000 K, and so densities are significantly less than air. Pyroclastic flows from volcanic eruptions often take the form of gravity currents. The density within the flow is a result of suspended ash and hot rocks, and is often many times larger than the surrounding air.

The first experiments on non-Boussinesq gravity currents were with air and water (Gardner & Crow 1970; Wilkinson 1982; Baines, Rottman & Simpson 1985), but more recently a few laboratory experiments covering the entire range of density differences have been reported by Keller & Chyou (1991) and Gröbelbauer, Fanneløp & Britter (1993). The working fluids in these latter experiments were a gas and a liquid or some combination of exotic gases.

Even in the simplest idealized situation in which the effects of friction can be ignored, there remains a dispute over what the speeds and depths of the two counterflowing gravity currents should be. For the Boussinesq case, Yih (1965) proposed that the depths of the two currents are equal and have the value of half the channel depth along their entire lengths, and that the speeds of both gravity currents are the same and have the value of Benjamin (1968)'s energy-conserving gravity current speed.

Klemp *et al.* (1994) have argued, based on shallow-water theory, that the idealized energy-conserving gravity current first proposed by Benjamin (1968) cannot be realized in the lock-exchange initial-value problem. Their reasoning is that the speed of this current would be faster than the fastest characteristic speed in the channel predicted from shallow-water theory. They argue that the inviscid gravity current depth can never be greater than 0.3473 of the channel depth, at which depth, according to Benjamin's theory, the gravity current has its fastest speed. Although they were mainly concerned with Boussinesq fluids, they commented that their arguments carry over to the extreme case of air and water.

However, the air and water experiments of Gardner & Crow (1970), Wilkinson (1982) and Keller & Chyou (1991) clearly show that the air cavity has both the shape and speed, when surface tension and viscous boundary-layer effects are taken into account, predicted by Benjamin's energy-conserving gravity current. Klemp *et al.* (1994) argue that the differences in speeds between the fastest allowable current and Benjamin's energy-conserving current are too small to discriminate in an experiment. This may be true, but the difference in current height is measurable and the measurements come much closer to the energy-conserving value than to the fastest allowable gravity current. Furthermore, the fastest allowable gravity current is also the current with the most dissipation, and the experimental results show very little in the way of dissipation for the air cavity propagating into water. Shin *et al.* (2004) have shown that energy-conserving gravity currents are generated by Boussinesq lock-exchange flows. Therefore, we conclude that despite the theoretical appeal of Klemp *et al.* (1994) arguments, previous large-density-difference and Boussinesq lock-exchange experiments do not support them.

Keller & Chyou (1991) formulated a hydraulic theory for the complete density ratio range. Their theory assumes that for small density differences both gravity currents

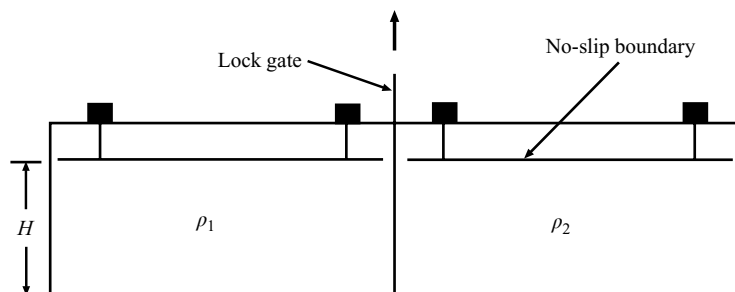


FIGURE 1. A sketch of the lock-release tank, showing two fluids of densities ρ_1 and ρ_2 , each having a depth of H and separated by a removable lock gate. The tank was fitted with a rigid lid to make the boundary conditions identical at the top and bottom of the tank.

are energy conserving and they are connected by a combination of a long-wave of expansion and an internal bore. For large density differences, they assume that the light current is energy conserving and the heavy current is dissipative and that the gravity currents are connected only by a long-wave of expansion. Attempts to validate this theory with experimental observations have so far been incomplete. Keller & Chyou's (1991) comparisons of their theory with their own experimental results are complicated by the small scale of their experiments which makes viscous effects and (for the case of immiscible fluids) surface tension important. A comparison between Keller & Chyou's (1991) theory with the experiments of Gröbelbauer *et al.* (1993) are also inconclusive. In particular, it is unclear from these experiments if, in fact, a bore exists in any of the observed flows.

In the present study, we discuss the lock-exchange problem over the full density difference range. We carry out a derivation of the theory proposed by Keller & Chyou (1991), discussing at length the different theories that can be used to describe the internal bore and we discover that there is another solution of the lock-exchange problem that involves only an expansion wave connecting the two gravity currents over the full range of density ratios. We perform laboratory experiments on both Boussinesq and non-Boussinesq gravity currents at high Reynolds numbers. The results of our experiments and those of the two-dimensional high-resolution numerical simulations described in a companion paper, Birman, Martin & Meiburg (2005, hereinafter referred to BMM), indicate that the theory without the bore gives the best agreement.

In §2, we describe the experimental techniques and present some qualitative as well as some representative quantitative results. In §3, we derive two hydraulic theories for the lock-exchange flow. A comparison between the theory, experiments and numerical simulations is given in §4. A stability analysis of both the heavy and light current fronts is reviewed in §5 to explain the observed striking differences in the stability of these two interfaces. A summary and discussion of the main results is given in §6.

2. Experiments

A schematic diagram of the lock exchange apparatus is shown in figure 1. Fluid of density ρ_1 is separated by a vertical barrier at the mid-point of a rectangular channel from fluid of density ρ_2 , with $\rho_1 > \rho_2$. The channel was 182 cm long, 23 cm wide and was filled to a depth of $H = 20$ cm. The upper boundary consisted of two sheets of Plexiglas in contact with the fluid surface, and separated by a thin gap to allow

Run	$\gamma = \rho_2/\rho_1$	ρ_1 (g cm ⁻³)	$U_L/\sqrt{(1-\gamma)gH}$	$U_H/\sqrt{(\gamma^{-1}-1)gH}$	Re
NaCl runs					
A	0.993	1.0051	0.43	0.45	10 800
B	0.974	1.0247	0.43	0.46	21 200
C	0.953	1.0477	0.42	0.42	26 600
D	0.950	1.0507	0.41	0.43	28 200
E	0.907	1.1000	0.45	0.48	43 200
F	0.870	1.1468	0.46	0.48	52 200
NaI runs					
G	0.701	1.4243	0.46	0.48	89 400
H	0.681	1.4663	0.46	0.49	95 500
I	0.677	1.4742	0.47	0.48	94 000
J	0.661	1.5106	0.46	0.50	102 400
K	0.647	1.5418	0.48	0.50	104 800
L	0.619	1.6111	0.50	0.49	108 400
M	0.607	1.6432	0.43	0.49	110 800

TABLE 1. Experimental parameters and measured values of U_L and U_H . The water depth $H = 20$ cm in all runs.

the lock gate to be removed. The flow was started by rapidly removing the lock gate vertically through the gap.

The flow was visualized using a shadowgraph, created by covering the face of the tank with tracing paper and positioning two 300 W projectors evenly spaced 4 m behind the tank. Video and still photographs were taken of the flow, which were used to measure the depths and front positions of the gravity current interface. The video images were digitized with a spatial resolution of 580 pixels in the horizontal and 350 pixels in the vertical, giving a spatial resolution of about 0.5 cm for a 180 cm horizontal field of view. The time resolution was 1/30 s.

The less dense fluid ρ_2 was freshwater and the denser fluid ρ_1 was either a solution of sodium chloride (NaCl) or sodium iodide (NaI). After exposure to air, a sodium iodide solution becomes slightly yellow, and this colouration can be observed in the images. For the sodium chloride runs with slight density differences (and consequently slight refractive index differences), blue food dye was added to distinguish the two fluids. With these solutes, density ratios $\gamma = \rho_2/\rho_1$ in the range $0.6 < \gamma < 1$ were achieved. Densities were measured using a density meter with an accuracy of 10^{-5} g ml⁻¹. The experimental parameters are given in table 1. The Reynolds number $Re = UH/\nu$, is based on the speed of the heavy current, the depth of the channel and the kinematic viscosity of fresh water (0.01 cm² s⁻¹). The values of Re achieved in these experiments are considerably larger than those obtained in previous experiments.

Results of two typical experiments are shown in figures 2 and 3. These figures show a series of shadowgraph images and plots of the positions of the light and heavy fronts for two density ratios. Figure 2 shows a Boussinesq case $\gamma = 0.993$ and figure 3 shows a non-Boussinesq case $\gamma = 0.681$. In both graphs the distance is plotted in units of the fluid depth, and time is non-dimensionalized by $\sqrt{H/g'}$, based on the reduced gravity $g' = g(1-\gamma)$ and the fluid depth H . Note that there is some blurring of the fronts owing to parallax since the camera is stationary and not moving with the fronts. The front positions were determined by analysing the digital images, based in relation to reference marks on the front of the tank. We estimate that the maximum error due to this parallax effect is about 0.5 cm.

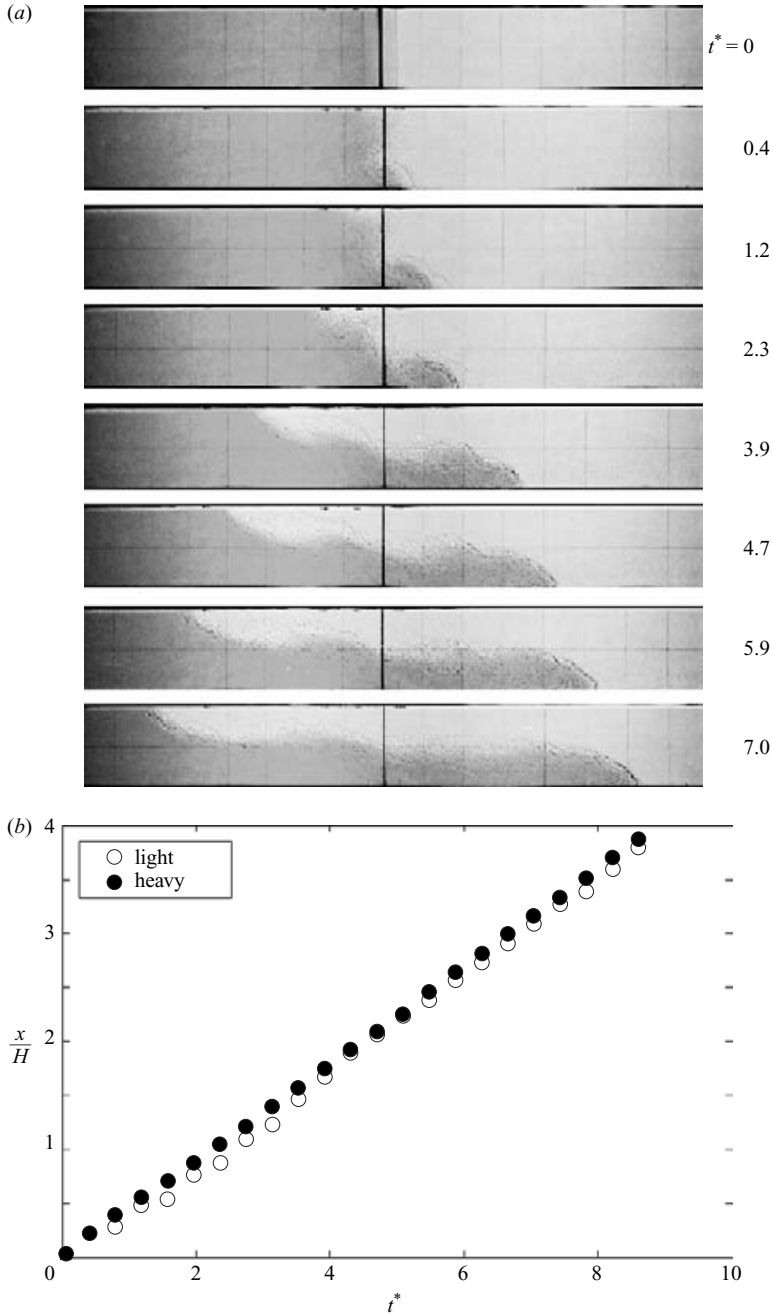


FIGURE 2. A Boussinesq lock exchange flow with $\gamma = 0.993$: (a) a sequence of shadowgraph images, and (b) a plot of the horizontal position relative to the position of the lock gate of the heavy front (filled circles) and light front (open circles) as a function of time after the removal of the lock gate ($t = 0$ corresponds to the time when the lock gate completely left the water). In these plots $t^* = t\sqrt{g(1-\gamma)/H}$ is the dimensionless time. The error in measuring the front position is about 0.5 cm or 0.03 in non-dimensional units and the error in measuring the time is 1/30 s or 0.006 in non-dimensional units.

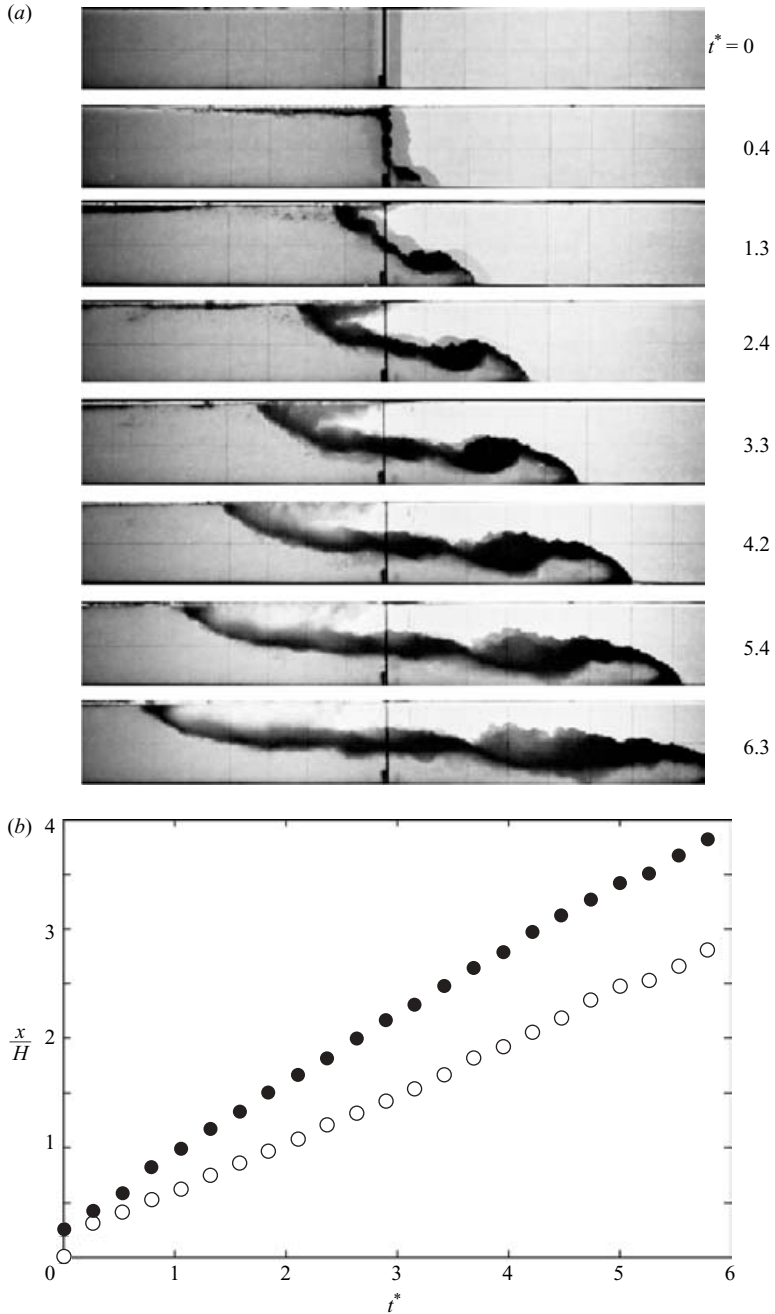


FIGURE 3. As for figure 2, but a non-Boussinesq lock-exchange flow with $\gamma = 0.681$. The non-dimensional time error is 0.04.

For the Boussinesq case in figure 2, the speeds of the light and heavy currents are constant and nearly the same. There is a slight offset as the vertical removal of the gate allows the heavy current to start first, but the slopes of the lines are indistinguishable within experimental accuracy. The flow is symmetrical about the centreline, with the leading part of each current occupying about half the depth. The

slight oscillations in the front position shown in figure 2 are due to sloshing in the tank caused by the removal of the lock gate.

For the non-Boussinesq case (figure 3), the speeds are again constant, but now the heavier current travels significantly faster than the light current. The light current travels at about the same non-dimensional speed as the Boussinesq current shown in figure 2. The symmetry of the Boussinesq case is lost, but the depths of the leading parts of the two currents are again close to the half depth of the fluid, with perhaps the heavy current front in this case slightly below this depth. The depth at the lock gate is close to mid-depth. Note that there is a patch of mixed fluid in the upper current just to the left of the gate position (most clearly seen at non-dimensional times 2.4 and 3.3). This is the result of mixing induced by imperfect gate removal. The gate was removed by hand which for the non-Boussinesq cases required considerable dexterity because of the very rapid motion of the currents. A similar mixed region does not appear in the Boussinesq case because the currents move much more slowly and, accordingly, made the gate removal easier to control.

In addition to the different speeds in the non-Boussinesq case, there is another significant asymmetry shown in figure 3. This is the formation of a region behind the heavy current front where there is a significant decrease in the depth of the dense layer. Associated with this is evidence of turbulence and mixing – see times $t^* > 3.3$ in figure 3.

It is clear that the symmetric flow seen in the Boussinesq case (figure 2) violates volume conservation if the two layers have the same depths but different speeds. In the non-Boussinesq case (figure 3), the volume flux carried to the right by the heavy layer would be greater than that carried to the left by the light layer. Hence the depth of the dense layer must decrease, as observed, to conserve volume. The experiments show that both the heavy and light fronts are moving at constant speeds with the depth of the light current downstream of the front close to half the channel depth, while the depth of the heavy current downstream of the front is shallower.

3. A theory for lock exchange flows

For Boussinesq fluids, both gravity currents in a lock exchange flow propagate at very nearly the same speed and have the same depth. For non-Boussinesq flows, the heavy current propagates faster than the light current and conservation of volume requires that the interface depth cannot be constant between the two fronts. In hydraulic theory, the change in interface depth can be accounted for by an expansion wave, a hydraulic jump or both. Keller & Chyou (1991), based on observations of their laboratory experiments, suggest that there are two possible flow configurations for the non-Boussinesq lock-exchange flow. These two possible flows are sketched in figure 4. The flow configuration illustrated in figure 4(a) is observed when $\gamma^* < \gamma \leq 1$ and that in figure 4(b) when $0 < \gamma \leq \gamma^*$, in which γ^* is a critical density ratio which is, as yet, to be determined.

In figure 4(a), a light energy-conserving gravity current of depth $h_L = H/2$ propagates to the left along the top of the channel with speed U_L , given by (3.1), and a heavy energy-conserving gravity current of depth $h_H = H/2$ propagates to the right with speed U_H , given by (3.3). Connecting these two gravity currents is a combination of a long wave of expansion and a two-layer bore (or hydraulic jump). The bore propagates to the right with speed C_B , with $C_B < U_H$, and has an upstream depth (where it joins with the expansion wave) of h_B . The speed of the bore relative to the heavy current speed is assumed to increase as γ decreases such that when $\gamma = \gamma^*$ the

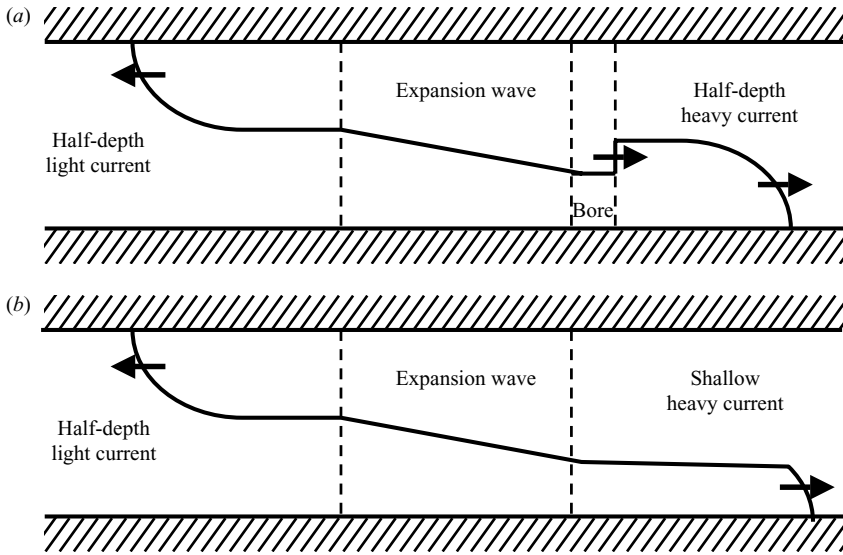


FIGURE 4. A schematic diagram of the two categories of lock-exchange flows: (a) a left-propagating energy-conserving light current and a right-propagating energy-conserving heavy current, connected by a long wave of expansion and a bore, and (b) a left-propagating energy-conserving light current and a right-propagating dissipative heavy current, connected by an expansion wave.

two speeds are the same. Any further decrease in γ produces the flow configuration shown in figure 4(b).

In figure 4(b), a light energy-conserving gravity current propagates to the left along the top of the channel with speed U_L and depth h_L , as in the previous case, but the heavy current propagating to the right along the bottom of the channel has a dissipative current front with speed U_H , given by (3.30), for some depth h_H such that $0 < h_H < H/2$. In this case, the two gravity currents are connected by a simple long wave of expansion without a bore.

The quantitative aspects of the theory for these two flow configurations, including an estimate of the value of γ^* , are described in the following subsections. The main features of this theory are the description of the long wave of expansion and the two-layer bore.

Another possibility we have discovered, which Keller & Chyou (1991) did not describe, is that the flow configuration shown in figure 4(b) can apply for the full range of γ . This situation also is described in the following subsections.

3.1. Density ratios near unity: $\gamma^* < \gamma \leq 1$

Using Benjamin's energy-conserving gravity current theory, the speed and height of the left-propagating current in figure 4(a) are given by

$$U_L = \frac{1}{2} \sqrt{(1-\gamma)gH}, \quad (3.1)$$

$$h_L = \frac{1}{2}H, \quad (3.2)$$

and the speed and height of the right-propagating heavy current are

$$U_H = \frac{1}{2} \sqrt{\frac{(1-\gamma)}{\gamma}gH}, \quad (3.3)$$

$$h_H = \frac{1}{2}H. \quad (3.4)$$

A detailed derivation of these results can be found in Rottman & Linden (2001). Note that, since $\gamma < 1$, (3.1) and (3.3) imply that the heavy current travels faster than the light current, consistent with observations.

As described earlier, these two fronts are assumed to be connected by a long wave of expansion and an internal bore. In the following subsections, the expansion wave will be described first, followed by the internal bore.

3.1.1. Expansion wave

Following Rottman & Simpson (1983) and Keller & Chyou (1991) the shallow-water equations for two-layer flow with zero total volume flux can be reduced to two partial differential equations for u_1 and h_1 , the fluid speed and depth of the lower layer,

$$\frac{\partial h_1}{\partial t} + h_1 \frac{\partial u_1}{\partial x} + u_1 \frac{\partial h_1}{\partial x} = 0, \quad (3.5)$$

$$\frac{\partial u_1}{\partial t} + a \frac{\partial u_1}{\partial x} + b \frac{\partial h_1}{\partial x} = 0, \quad (3.6)$$

in which

$$a = \frac{u_1(h_2 - \gamma h_1) + 2\gamma u_2 h_1}{(\gamma h_1 + h_2)}, \quad (3.7)$$

$$b = \frac{-\gamma(u_1 - u_2)^2 + (1 - \gamma)gh_2}{(\gamma h_1 + h_2)}, \quad (3.8)$$

where u_2 and h_2 are the fluid speed and depth of the upper layer,

$$h_2 = H - h_1, \quad (3.9)$$

$$u_2 = -\frac{u_1 h_1}{h_2}. \quad (3.10)$$

The partial differential equations (3.5) and (3.6) can be expressed in the characteristic form

$$\frac{du_1}{dh_1} = \frac{b(x, t)}{u_1(x, t) - \lambda_{\pm}(x, t)} \quad (3.11)$$

on

$$\frac{dx}{dt} = \lambda_{\pm}, \quad (3.12)$$

in which λ_{\pm} are the characteristic speeds

$$\lambda_{\pm} = \frac{1}{2}(a + u_1) \pm \frac{1}{2}[(a + u_1)^2 - 4(au_1 - bh_1)]^{1/2}. \quad (3.13)$$

With this formulation we can obtain the fluid speed in the lower layer as a function of the lower-layer depth by integrating (3.11) from the left-propagating energy-conserving solution, where $h_1 = H/2$, to $h_1 = 0$ along the λ_+ characteristic. The actual values of h_1 and u_1 at the endpoints of this calculation are determined by matching this solution with either the internal bore, described in § 3.1.3, or directly with the dissipative gravity current front condition, as described in § 3.2.

A plot of u_1 as a function of h_1 computed in this way, for various values of γ , is shown in figure 5. As shown in this figure, the fluid speed in the lower layer increases as the lower-layer depth decreases. Also, we find that λ_+ becomes imaginary for some values of h_1 when $0.95 \lesssim \gamma < 1$. In the figure, the curves stop when λ_+ becomes

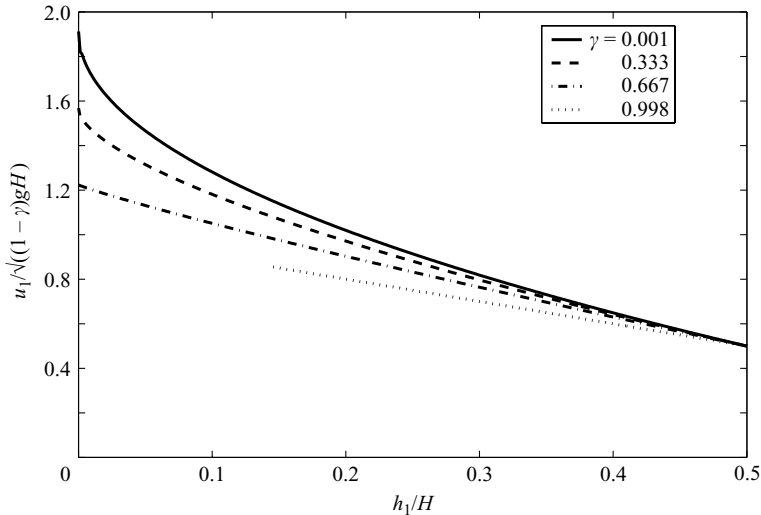


FIGURE 5. The speed u_1 of the fluid in the lower layer in the expansion wave as a function of the lower layer depth h_1 for $\gamma = 0.001, 0.333, 0.667$ and 0.998 . The characteristic speed λ_+ is imaginary for values of h_1 where no values of u_1 are plotted.

imaginary. As can be seen, λ_+ becomes imaginary for small h_1 when $\gamma \approx 0.95$, and the range of h_1 over which λ_+ is imaginary increases as $\gamma \rightarrow 1$, such that λ_+ is imaginary for all h_1 when $\gamma = 1$. An imaginary λ_+ implies that the interface is unstable. The stability of the interface is discussed in more detail in § 5.

3.1.2. Internal bore

To complete the description of the flow shown in figure 4(a), we have to patch a two-layer internal bore between the right-propagating expansion wave and the right-propagating energy-conserving heavy current front. This requires a hydraulic theory for a two-layer bore that propagates into a shear flow.

As described, for example, in § 3.5 of Baines (1995), the application of the principles of conservation of mass in each layer and the overall conservation of momentum through the jump does not produce a closed problem, as it does in the limiting case of a free-surface hydraulic jump. This is because it is unclear how the necessary energy dissipation should be distributed between the two layers. There have been several attempts to resolve this ambiguity within the context of hydraulic theory.

Yih & Guha (1955) close the problem by making the additional assumption that the pressure remains hydrostatic through the jump. This theory predicts an overall energy loss through the jump, although, as shown by Wood & Simpson (1984), one of the layers experiences an energy gain. Numerical simulations and laboratory experiments, as described, for example, in Baines (1995) have confirmed that this theory is valid for small-amplitude bores propagating into two-layer fluids at rest, but is inadequate for larger-amplitude bores.

Chu & Baddour (1977) and independently Wood & Simpson (1984) proposed that a better approximation would be to replace the assumption that the pressure is hydrostatic through the bore with an assumption about energy conservation in each fluid layer through the bore. Specifically, they assumed that the energy must be conserved in the contracting layer and that energy must be lost in the expanding layer. This idea is based on earlier results of hydraulic flow in a one-layer fluid

with boundary-layer, separation. This new theory produced results that are almost indistinguishable from those of Yih & Guha (1955) and in particular the new theory was not any better at predicting large-amplitude bores. Lane-Serff, Beal & Hadfield (1995) successfully used this approach to develop a theory for two-layer bores propagating into a shear flow established by a gravity current.

Keller & Chyou (1991) proposed a model for a two-layer bore propagating into a shear flow produced by a lock-exchange flow. In their model, the hydrostatic pressure assumption is replaced with the assumption that the difference between the static pressures upstream and downstream of the bore is proportional to the difference between the stagnation pressures upstream and downstream of the bore. The constant of proportionality, Λ , was argued on physical grounds to have values in the range $0 < \Lambda \leq 1$.

Klemp, Rotunno & Skamarock (1997) suggested that the assumption of energy conservation in the expanding layer and energy dissipation in the contracting layer is consistent with the Benjamin (1968) theory of gravity currents in the limit of very large-amplitude bores. This assumption is opposite to that of Chu & Baddour (1977) and Wood & Simpson (1984), but it is the same as the theory proposed by Keller & Chyou (1991) when $\Lambda = 1$. Lane-Serff & Woodward (2001) applied this theory to internal bores produced by exchange flows over sills. Klemp *et al.* (1997) gave physical arguments for why their theory should be approximately correct for bores propagating into a fluid at rest. Similar arguments suggest that this theory will not be accurate for bores that are propagating into a shear flow, as would be the case for a two-layer hydraulic jump that forms in the lee of a hill. In this case, the upstream vorticity field makes the internal jump behave more like the hydraulic jump in a free-surface flow.

In the present work, we implemented all the theories described above to represent the bore that is assumed to exist in the non-Boussinesq lock-exchange flow. In most cases, we found only small differences between the results of the different theories. The largest differences were between the theories that assume all the energy is dissipated either in the expanding layer or the contracting layer. Here, for brevity, we will limit discussion to these two theories. We will derive the theory for non-Boussinesq fluids with an upstream shear flow using either assumption, and use these results to bound the possible outcomes, particularly to bound the possible values for γ^* . We note that it is possible, though unlikely, that these existing theories do not bound all the possible flows.

Figure 6 shows a sketch of the two-layer bore and the heavy gravity current front. This figure defines the nomenclature used in this section. In particular, note that P_A and P_B are the pressures at the top of the channel at stations upstream and downstream of the bore, respectively, and that p_A and p_B are the pressures on the bottom of the channel, related to the pressures at the top of the channel by the hydrostatic relations:

$$p_A = P_A + \rho_1 g h_A + \rho_2 g (H - h_A) \quad (3.14)$$

and

$$p_B = P_B + \rho_1 g h_B + \rho_2 g (H - h_B). \quad (3.15)$$

The conservation of mass in each layer and the conservation of horizontal momentum of the fluid moving through the bore requires

$$(u_A - C_B)h_A = (U_H - C_B)h_H, \quad (3.16)$$

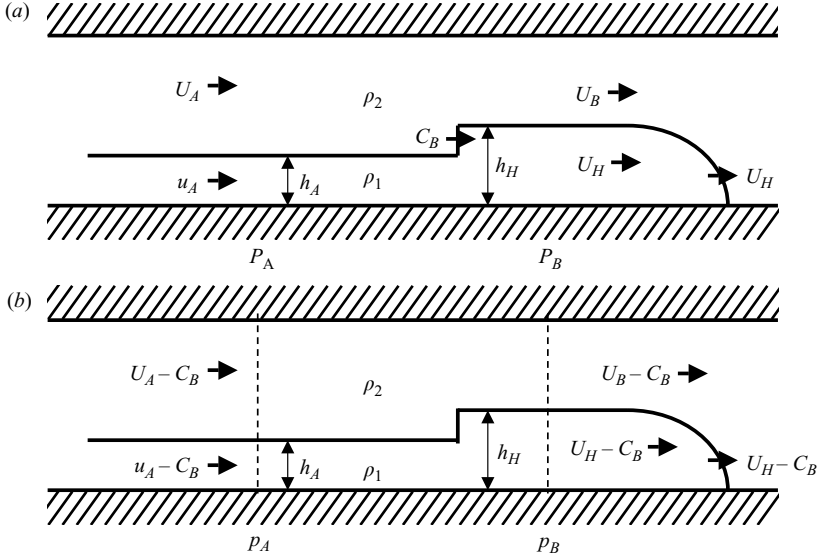


FIGURE 6. A sketch of the right-propagating two-layer bore and the right-propagating energy-conserving heavy front: (a) in the laboratory reference frame and (b) in the reference frame in which the bore is at rest. In (b), the vertical dashed lines represent the upstream and downstream edges of the control volume over which the integral form of the horizontal momentum equation is applied, as described in §3.1.2.

$$(U_A - C_B)(H - h_A) = (U_B - C_B)(H - h_H), \quad (3.17)$$

and

$$\begin{aligned} \frac{1}{\rho_1}(P_B - P_A)H &= \frac{1}{2}(1 - \gamma)g(h_A^2 - h_H^2) \\ &+ (u_A - C_B)^2 h_A - (U_H - C_B)^2 h_H \\ &+ \gamma[(u_A - C_B)^2(H - h_A) - (U_B - C_B)^2(H - h_H)]. \end{aligned} \quad (3.18)$$

Given U_H and h_H , we can use these three equations to determine u_A , h_A and C_B if we can specify an additional equation for the pressure drop across the bore.

As we discuss above, the determination of the pressure drop across a two-layer bore has been a source of controversy, because it is unclear how the necessary energy dissipation should be distributed between the two layers. Since this issue remains unresolved, we will consider the two extreme cases as a way of bounding the possible solutions.

Chu & Baddour (1977) and independently Wood & Simpson (1984) make the assumption that all the energy dissipation occurs in the expanding layer, which is the lower layer in our case, so that energy in the contracting layer is conserved. Using this approximation in the present case, we can use Bernoulli's equation along the top of the channel to obtain a relationship for the pressure drop across the bore,

$$\frac{1}{\rho_1}(P_B - P_A) = \frac{1}{2}\gamma(U_H - C_B)^2 \left[\frac{1/4}{H - h_A} - H \right]. \quad (3.19)$$

Substitution of (3.19) into (3.18) and the use of (3.16) and (3.17) to eliminate the other variables produces a single quadratic equation for C_B

$$q(1 - 2\sqrt{\gamma}C_B^*)^2 + r(1 + 2\sqrt{\gamma}C_B^*)^2 + s = 0, \quad (3.20)$$

where

$$q = \frac{1}{\gamma} \left(\frac{1}{2} \frac{H}{h_A} - 1 \right), \quad (3.21)$$

$$r = \frac{1}{2(1 - h_A/H)} \left[1 - \frac{1}{2(1 - h_A/H)} \right], \quad (3.22)$$

$$s = 4(h_A^2/H^2 - 1), \quad (3.23)$$

and

$$C_B^* = \frac{C_B}{\sqrt{(1 - \gamma)gH}}. \quad (3.24)$$

Klemp *et al.* (1997) make the opposite assumption, considering the best approximation to be that all the energy is dissipated in the contracting layer, which is the upper layer in the present case. In this case, we can use Bernoulli's equation along the bottom of the channel to obtain the relation

$$\frac{1}{\rho_1}(p_B - p_A) = \frac{1}{2}[(u_A - C_B)^2 - (U_H - C_B)^2]. \quad (3.25)$$

Using the hydrostatic relations (3.14) and (3.15) to relate p_A and p_B to P_A and P_B , respectively, and substituting into (3.18), (3.16) and (3.17), we obtain again an equation of the form (3.20), but with the coefficients given by

$$q = \frac{1}{\gamma} \left(\frac{1}{2} \frac{H}{h_A} - 1 \right) - \frac{1}{\gamma} \left(\frac{H^2}{4h_A^2} - 1 \right), \quad (3.26)$$

$$r = \frac{1}{2(1 - h_A/H)} - 1, \quad (3.27)$$

$$(3.28)$$

and

$$s = 4(1 - h_A/H)^2 - 1. \quad (3.29)$$

Equation (3.20) is a simple quadratic equation that is easy to solve for C_B^* as a function of h_A/H .

3.1.3. Matching

In order to determine the strength and speed of the bore in this flow, we have to match u_A and h_A of the bore with u_1 and h_1 from the expansion wave. Plots of u_A and u_1 as functions of h_1 (setting $h_A = h_1$) are shown in figure 7. Where these curves intersect are solutions that patch the expansion wave to the two-layer bore.

A plot of the bore speed predicted in this way, for each of the two theories, is plotted in figure 8 as a function of γ . Also plotted in this figure is the speed of the heavy energy-conserving gravity current front. Note that the bore speed predicted by the theory based on the approximations made by Wood & Simpson (1984) is slower than the gravity current speed except at $\gamma = 0$ where it equals the gravity current speed. The bore theory based on the approximations of Klemp *et al.* (1997), on the other hand, is slower than the gravity current speed for high density ratios $0.3 \lesssim \gamma < 1$, and greater than the gravity current speed for low density ratios $0 < \gamma \lesssim 0.3$. In this latter case, our hypothesized form of the lock-exchange flow depicted in figure 4(a) must be wrong, and the lock exchange flow must have the form depicted in figure 4(b).

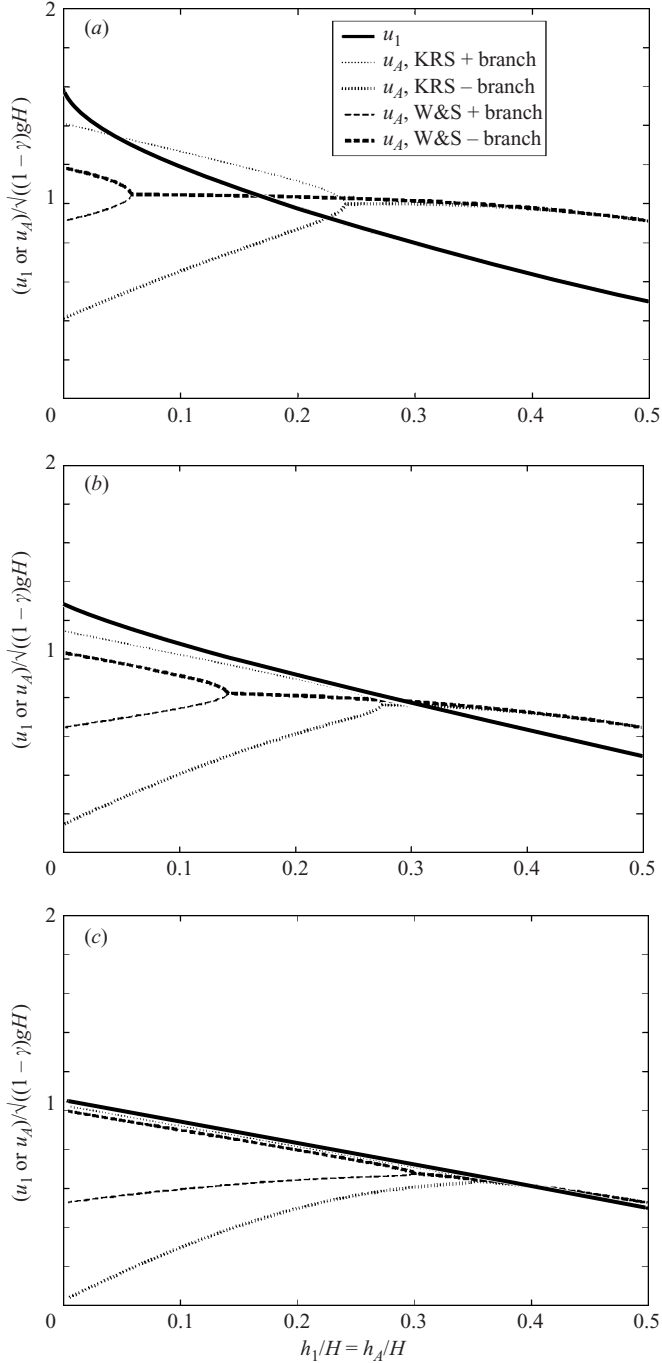


FIGURE 7. The speed u_1 in the expansion wave (from figure 5) and the speed u_A downstream of the bore at depth $h_1 = h_A$. The solid line is the fluid speed in the expansion wave, the dashed lines are the speeds of the bore according to the theory of Klemp *et al.* (1997, KRS) and the dotted lines are from the theory of Wood & Simpson (1984, W&S) (for both theories, thin line widths represent the positive branches and thick line widths the negative branches of the theoretical solutions): (a) $\gamma = 0.30$, (b) $\gamma = 0.60$ and (c) $\gamma = 0.90$.

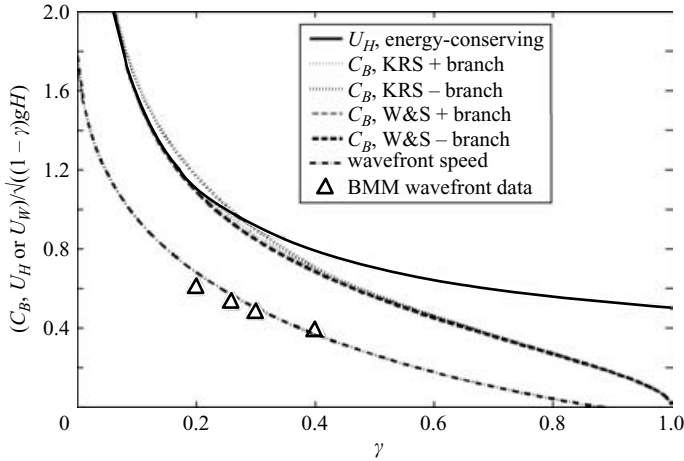


FIGURE 8. A plot of the bore speed C_B as computed using the theory of Klemp *et al.* (1997, KRS) (dotted lines, thin for positive branch and thick for negative branch) and using the theory of Wood & Simpson (1984, W&S) (dashed lines, thin for positive branch and thick for negative branch) compared with U_H the heavy energy-conserving gravity current speed (solid line). The negative branch solution of Klemp *et al.* (1997) intersects the gravity current speed curve at $\gamma = 0.2810$, whereas all the other bore speed curves intersect the gravity current speed at $\gamma = 0$, although they remain very close to this curve for $\gamma < 0.2$. Also plotted in this figure as a dash-dot line is the theoretical expansion wave-front speed, as well as measurements of this speed from the numerical simulations of BMM (triangles).

Since we do not know which bore theory is most correct in this shear-flow situation, we can say only that the transition from one form of the lock-exchange flow to the other, if it occurs, occurs for some value of $\gamma = \gamma^*$ in the range $0 < \gamma^* \lesssim 0.3$.

3.2. Density ratios near zero: $0 < \gamma \leq \gamma^*$

The structure of the flow in this regime is depicted in figure 4(b). In this case, the expansion wave is patched to one of Benjamin's dissipative gravity current fronts directly. The speed of this kind of front as a function of the current depth h_H is given by the formula

$$U_H = \sqrt{(1-\gamma)gH} \left[\frac{1}{\gamma} \frac{h_H}{H} \left(2 - \frac{h_H}{H} \right) \frac{1 - h_H/H}{1 + h_H/H} \right]^{1/2}. \quad (3.30)$$

We can determine the matching conditions by calculating U_H from (3.30) as a function of $h_H/H = h_1/H$, and comparing the values with the speeds shown in figure 5. In this case, the current adjusts to carry the flux supplied from the rear.

4. Results

The values we measured for the speed of the light current over a range of density ratios are shown in figure 9. Included in figure 9 are results from other experiments and also the numerical simulations of BMM which cover a larger range of density ratios than we were able to achieve in our experiments. Our Reynolds numbers are much higher than those achieved in the previous experiments (mainly because their lock-exchange tanks were much smaller) and generally higher than obtained in the numerical simulations. Based on the observed speed and depth of the channel, the Reynolds numbers Re in our experiments varied from 10000 for the

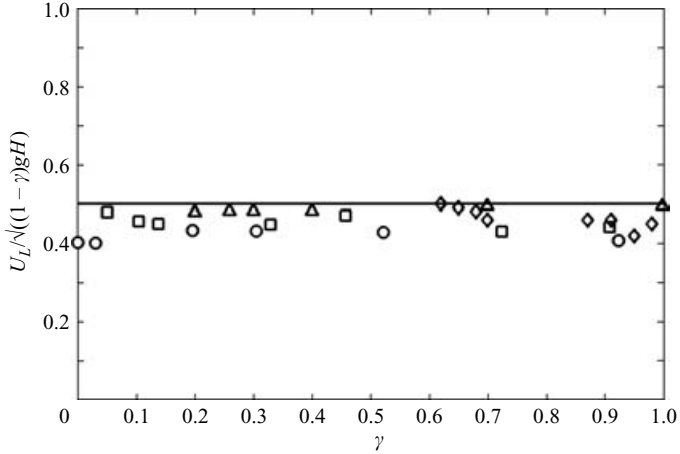


FIGURE 9. The light current: a comparison of the theoretical front speed U_L , as a function of the density ratio γ , with measured values in the laboratory and computed values from the direct numerical simulations of BMM. The theoretical energy-conserving speed given by (3.1) is plotted as a solid line and the measured values as symbols. \diamond , present experimental results; \square , Gröbelbauer *et al.* (1993) results; \circ , Keller & Chyou (1991) results; \triangle , BMM numerical simulations.

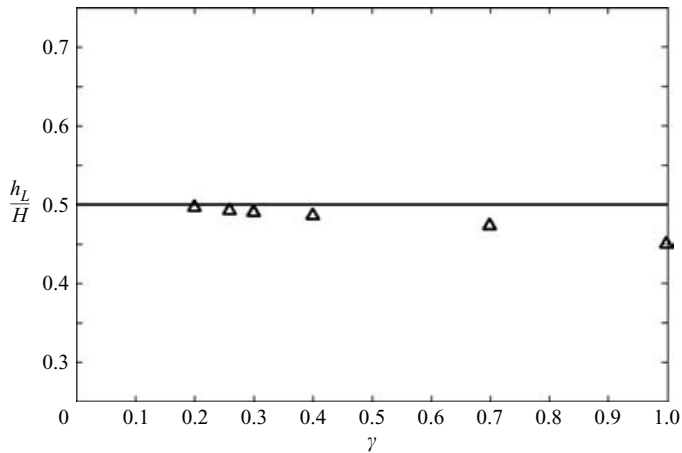


FIGURE 10. The light current: a comparison of the theoretical front height h_L (solid line), as a function of the density ratio γ , with computed values (triangles) from the numerical simulations of BMM.

Boussinesq currents to over 100 000 for the non-Boussinesq currents (see table 1). The results of our experiments are consistent with the earlier experiments and with the numerical simulations, showing that, over this Reynolds-number range, the speeds are independent of Re and the energy-conserving front speed (3.1) fits the measured front speed well, over the full range of γ .

The heights of the light currents determined from the numerical simulations of BMM are compared with the theoretical front height in figure 10. (Unambiguous measurements of the current height are difficult to make in experiments. Our qualitative observations are consistent with the theoretical values, but we do not have quantitative information from our own or from other experiments.) The agreement

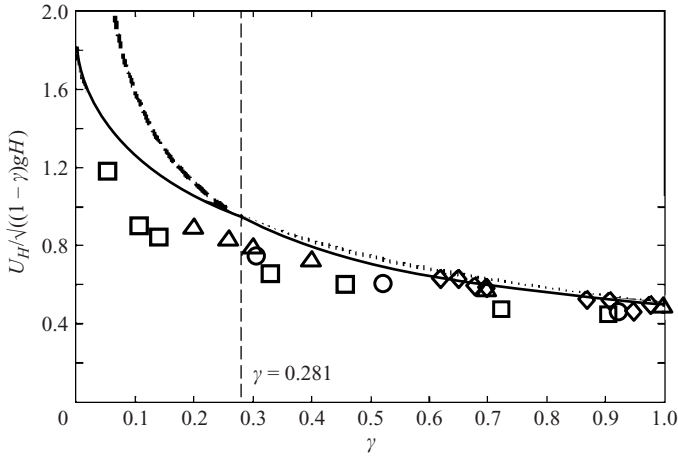


FIGURE 11. The heavy current: a comparison of the theoretical front speeds, as a function of the density ratio γ , with measured values in the laboratory and computed values from the numerical simulations of BMM. The theoretical results are plotted as lines and the measured values as symbols. The energy-conserving theory is plotted as a dashed line, the theory of Keller & Chyou (1991) (using the negative branch of the Klemp *et al.* (1997) internal bore theory) is plotted as a solid line, and the theory using only a dissipative gravity current and expansion wave as a dotted line. \diamond , the present experimental results; \square , Gröbelbauer *et al.* (1993) results; \circ , Keller & Chyou (1991) results; \triangle , BMM numerical simulations.

is good over the full range of density ratios. The observed speeds are generally a few per cent below the theoretical prediction, and this discrepancy is believed to be a result of dissipation at the top and bottom boundaries and mixing at the interface. The results from the numerical simulations for the height are remarkably close to the theoretical value, except near $\gamma = 1$. The light current interface is observed, in both the experiments (see figure 3a) and the numerical simulations (see figure 5 of BMM), to be stable with little mixing for all values of γ away from $\gamma = 1$. We suspect that the mixing that does occur for γ near unity has contaminated the height measurements in that parameter regime. Further comments about the interface stability are given in §5.

The values we measured for the speed of the heavy current over a range of density ratios are shown in figure 11 and the numerical values for the heights of the heavy current are shown in figure 12. Again, results from other experiments as well as from the numerical simulations of BMM are included in these figures. As for the light current, the experimental and numerical values for the speed of the heavy current are in good agreement with the hypothesized theory, both with and without the bore, but they clearly are not consistent with the energy-conserving theory for small values of γ . Note that the difference between the theory with and without the bore is smaller than the experimental error and so we cannot use the measurements of the gravity-current front speed alone to determine which of these theories is the correct one.

The predicted speed of the expansion wavefront that connects with the heavy gravity current, as illustrated in figure 4(b), is plotted in figure 8. This speed is given by (3.13) evaluated with the speed and height of the heavy gravity current for each value of γ . As can be seen in the plot, this speed is always less than that of the heavy gravity-current front for all γ except $\gamma = 0$ where the two speeds are the same. We attempted to identify this expansion wavefront in the experiments and numerical

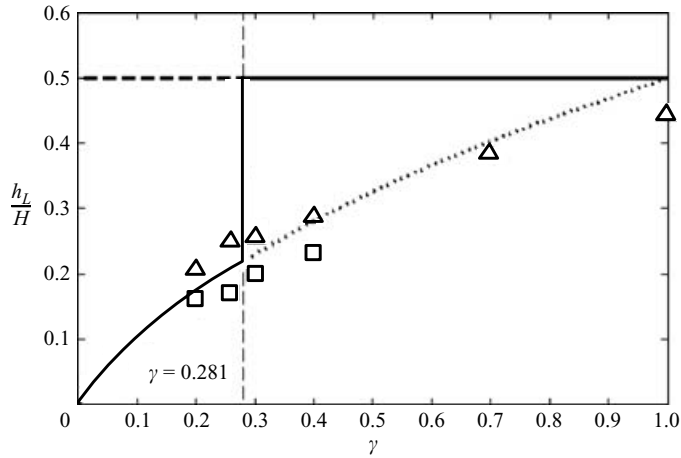


FIGURE 12. The heavy current: a comparison of the theoretical front height, as a function of the density ratio γ , with the computed values from the numerical simulations of BMM. The theoretical results are plotted as lines and the measured values as symbols. ---, the energy-conserving theory; —, the theory of Keller & Chyou (1991) (using the negative branch of the Klemp *et al.* (1997) internal bore theory); ..., the theory using only a dissipative gravity current and expansion wave. The numerical results of BMM are shown as triangles for the measured front height and squares for the measured height of the current where the expansion wave meets the gravity current.

simulations by associating it with the point where there is a sharp decrease in the heavy current interface, as can be seen in figure 3(a). This was easier to do with the numerical simulations than with the experimental results. The speeds obtained by plotting the position of this point as a function of time in the numerical simulations are plotted in figure 11 and show very good agreement with the theory. This result strongly suggests that the theory without the bore is more representative of the observations.

The plots of the heavy-current height strengthen the conclusion that the theory without the bore is more appropriate. In the experiments, the height of the heavy current is difficult to measure because of the mixing that occurs along the interface in the neighbourhood of the heavy front. However, in the numerical simulations, a quantitative measure of the interface height can be made, as described in BMM, and this result is plotted in figure 12. The plotted results are for the height of the heavy gravity current as well as the height of the interface at the point associated with the expansion wavefront. In the theory, these two heights should have the same value and the measured heights fall closely on either side of the theoretical curve. The results show that the numerical simulations are more in agreement with the theory without the bore than the one with the bore. Clearly, the height of the measured heavy current decreases steadily as γ decreases, and does not show the behaviour (i.e. the height is constant when $1 > \gamma > \gamma^*$) predicted by the theory that includes a bore.

Comparisons between the theoretical shape as calculated by Benjamin (1968) and the observed currents when $\gamma = 0.993$, 0.681 and 0.001 are shown in figure 13. The theoretical shape, which is strictly valid only near the front, has been extended by a straight horizontal line at mid-depth to join the two fronts. The agreement with the observed currents appears very good for the cases with $\gamma = 0.993$ and 0.681 and not very good for the case with $\gamma = 0.001$. Note that in this latter case, we show only the heavy current front in the photograph; the air cavity front that is off the

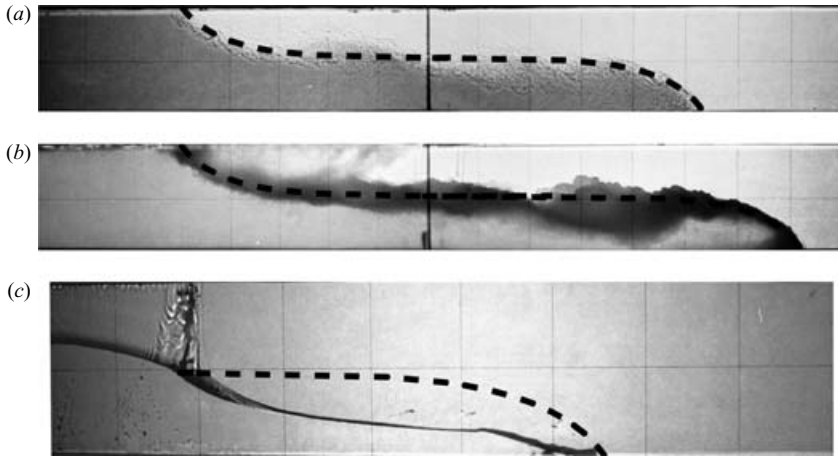


FIGURE 13. Shadowgraph images of lock-exchange flows for three different density ratio values: (a) $\gamma = 0.993$, (b) $\gamma = 0.681$ and (c) $\gamma = 0.001$. The dashed lines represent the theoretical shape of an energy-conserving gravity current. In the case with $\gamma = 0.001$, only the heavy current front is shown.

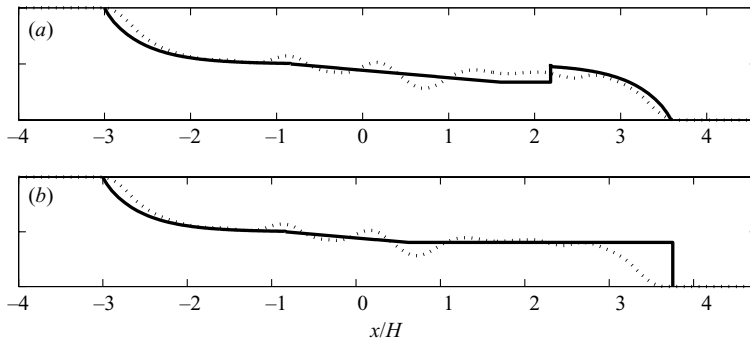


FIGURE 14. The theoretical interface shape (solid line) compared with the computed shape (dotted line) from the simulations by BMM for the case with $\gamma = 0.7$ at $t^* = 6.0$: (a) using the theory with a bore and (b) using the theory without a bore (note: there is no theory for the front shape of the dissipative current so a square front is shown in the diagram). Compare these two plots with figure 13(b).

left-hand side of the photograph is represented well by Benjamin’s energy-conserving current shape, as we know from previous studies (e.g. Wilkinson 1982). We would expect very good agreement for both fronts in the first case. In the second case, we expect the light current front to be represented well by the energy-conserving theory, but we expect the heavy current front height to be less than half the channel depth, as indicated in figure 12. Because of mixing at the interface it is difficult to make an undisputed estimate, but the heavy current front height in this case appears to be, on average, slightly less than half-depth. The last case, with $\gamma = 0.001$, is the dam-break problem for which we do not expect Benjamin’s energy-conserving theory to be valid for the heavy front.

A comparison of the full interface shape predicted by both theories, with and without the bore, with that obtained from the numerical simulations of BMM for the case with $\gamma = 0.7$ is shown in figure 14. With the large fluctuations of the interface

in the simulations, which are mostly an artefact of the two-dimensionality of the simulations, even for this value of γ , it is still difficult to determine which theory is the more correct. Note that in figure 14(b), the theoretical dissipative heavy front, for which there is no theory for the front shape, is represented as a rectangle.

5. Interface stability

As can be observed in figures 2(a) and 3(b), in general, the light gravity-current interface is more stable and has less mixing than does the heavy gravity-current interface, and this is especially true for the smaller values of γ . Similar differences between the light and heavy fronts are observed in the numerical simulations of BMM. Benjamin (1968) comments on this aspect of the lock-exchange flow and presents a linear stability theory that explains the observations. We briefly review his findings here and add a few additional results from the stability theory.

Benjamin (1968) considers two layers of fluid separated by a sharp density interface. The fluid velocity in each layer is assumed to be uniform and horizontal. The densities, depths and velocities are denoted by ρ_i , h_i and U_i , where $i = 1, 2$ correspond to the lower and upper layers, respectively. The undisturbed position of the interface is at $z = 0$ and the lower and upper boundaries are at $z = -h_1$ and $z = h_2$, respectively, with $H = h_1 + h_2$. The fluid is assumed to be inviscid, and the velocities are uniform so that the undisturbed flow is irrotational, except at the interface, which is a vortex sheet.

Consider a small perturbation of the interface of amplitude a of the form

$$\eta = ae^{i(kx - \omega t)} = ae^{ik(x - ct)}, \quad (5.1)$$

travelling in the x -direction with speed $c = \omega/k$, in which ω is the frequency and k is the wavenumber of the wave. A relationship between c and k can be found using potential theory in each layer and the linearized forms of the kinematic and dynamic boundary conditions at the interface. This relationship is given by

$$\rho_1 k(c - U_1)^2 \coth kh_1 + \rho_2 k(c - U_2)^2 \coth kh_2 - g(\rho_1 - \rho_2) = 0. \quad (5.2)$$

This is a quadratic equation for c . Instability of the interface is indicated by complex conjugate roots of this equation with $\text{Im}(c) > 0$, taking k to be positive and real. The requirement for this to be true is

$$\gamma \tanh(kh_1) + \tanh(kh_2) < \frac{\gamma}{1 - \gamma} \frac{(U_1 - U_2)^2}{g/k}. \quad (5.3)$$

For an energy-conserving light current

$$h_1 = h_2 = \frac{1}{2}H \quad (5.4)$$

and

$$(U_1 - U_2)^2 = (1 - \gamma)gH, \quad (5.5)$$

and instability occurs when

$$\tanh(kH/2) < \frac{\gamma}{1 + \gamma} kH. \quad (5.6)$$

Since $0 < \gamma < 1$ and k is taken as positive, this inequality is satisfied for a range of wavenumbers $k > k_c$, where k_c decreases as γ decreases, as illustrated in figure 15(a). Thus the interface is unstable to short waves, but stable to long-wave perturbations. For a cavity, when $\gamma = 0$, the interface is stable for all wavelengths.

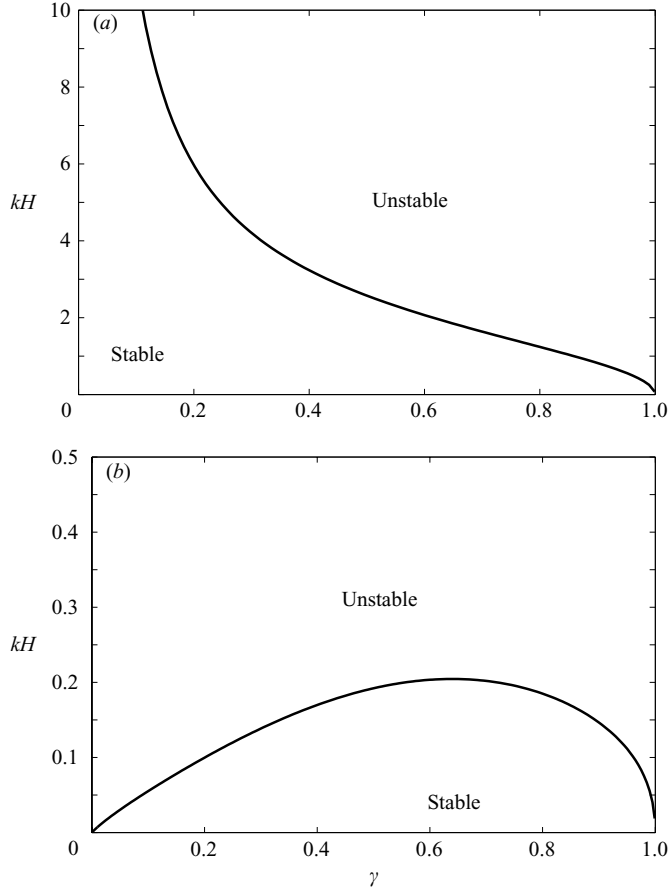


FIGURE 15. The wavenumber k_c as a function of the density ratio γ for which the gravity current interface is neutrally stable according to linear stability theory, which separates (k, γ) space into *stable* and *unstable* regions: (a) the light gravity current and (b) the heavy gravity current. Note the different vertical scales in (a) and (b).

For the heavy current in our lock-exchange flow

$$h_2 = H - h_1, \quad (5.7)$$

where h_1 is the depth of the current, and

$$(U_1 - U_2)^2 = g \frac{1 - \gamma}{\gamma} h_1 \left(2 - \frac{h_1}{H} \right) \left[1 - \left(\frac{h_1}{H} \right)^2 \right]^{-1}, \quad (5.8)$$

and instability occurs when

$$\gamma \tanh(kh_1) + \tanh[k(H - h_1)] < \left(2 - \frac{h_1}{H} \right) \left[1 - \left(\frac{h_1}{H} \right)^2 \right]^{-1}. \quad (5.9)$$

Using the relationship between h_1 and γ for the heavy current as determined in § 3 for the lock-exchange flow without a bore, this inequality is satisfied for the range of wavenumbers $k > k_c$, where k_c is plotted in figure 15(b). In this case, the interface is unstable to short waves, but stable for very long wave perturbations. When the lock

exchange is Boussinesq, $\gamma = 1$, or when it is a dam break, when $\gamma = 0$, the interface is unstable for all wavelengths.

These results imply that the interface above the heavy current is unstable to a larger range of wavelengths than the interface below the light current, especially in the non-Boussinesq (small γ) case. The reason for this difference is that, although the (stabilizing) density difference across the interface is the same, the higher speed of the dense current gives a greater shear across the interface. Our observations (figure 3*a*) are consistent with these predictions.

6. Conclusions

The results of an experimental and theoretical study of the non-Boussinesq lock-exchange problem have been presented. The experiments were performed in a rectangular channel using water and either a sodium iodide solution or a sodium chloride solution as the two fluids. These combinations of fluids have density ratios (light over heavy density) in the range 0.61 to 1. A two-layer hydraulic theory is developed to model the experiments. The theory assumes that a light gravity current propagates in one direction along the top of the channel and a heavy gravity current propagates in the opposite direction along the bottom of the channel. The theory assumes that the two currents are connected by either a combination of an internal bore and an expansion wave, or just an expansion wave. The present results and the results of two previous non-Boussinesq sets of lock-exchange experiments, both of which used two different gases or a gas and a liquid as the two fluids (with density ratios in the range 0.1 to 1), and with the two-dimensional numerical simulations (with density ratios in the range 0.001 to 1) of BMM are compared with the theory.

The conclusion from a comparison of the proposed theories with our experimental observations and the high-resolution, two-dimensional numerical simulations of BMM is that the theory in which the two gravity currents are connected by a simple wave of expansion without an internal bore is most representative of non-Boussinesq lock exchange flows. In this case, the light current is an energy-conserving gravity current that occupies half the depth of the channel for all values of γ , whereas the heavy current is what Benjamin (1968) calls a dissipative current with a height that decreases with decreasing γ . This conclusion contradicts the description of the non-Boussinesq lock-exchange flow given by Keller & Chyou (1991), who concluded that the heavy current is energy conserving and connected to the light current by an expansion wave and an internal bore for $0.3 \lesssim \gamma \leq 1$.

The theory developed here assumes that, at long times, there are two gravity currents connected by an expansion wave. The front conditions for the currents are analogous to hydraulic jump conditions, and they require a particular relationship between the local value of speed and height. These values have to adjust within these constraints in order to match up with the expansion wave. This matching ensures that mass and momentum are conserved. We assume that the light current is an energy-conserving Benjamin current that is locally steady. In taking this long-time approach, we have to abandon some information about how the flow sets itself up, and therefore have to postulate that the light current is energy conserving and steady.

It seems possible that both current fronts could be unsteady. In that case, the long-time solution procedure would break down since all parts of the flow would be unsteady. Fortunately, the experiments and numerical simulations show that our assumptions about the light current are approximately correct. Since the expansion wave connects the two fronts, it is, therefore, necessary for the heavy current to adjust

to the flux supplied to the lower layer from the rear. This flux is set by the light current and so the energy-conserving front controls the flow on both sides of the lock.

The model proposed in this paper of an energy-conserving light current connected to a dissipative dense current by an expansion wave is supported by calculations of the dissipation given in BMM. They show in their figure 13 that the fraction of the potential energy loss that is converted to dissipation increases with time and reaches a maximum of about 12% by the end of the simulation. In the Boussinesq case, the energy loss in the light and dense fluids is about the same (BMM, figure 10). Much of this dissipation is associated with the billows that form on the interface (which is why the fraction of the potential energy dissipated increases with time), and in the non-Boussinesq case is significantly larger, by a factor of about 4 for $\gamma = 0.2$, for the dense current (i.e. to the right-hand side of the lock) than for the light current (see BMM, figure 12). Thus the light front is close to energy conserving for all density ratios. Figure 16 of BMM also shows that the energy loss reduces with Re . Since our experiments are generally at much higher Reynolds numbers than the simulations, we expect the light front in the experiments to be close to energy conserving.

We acknowledge the productive collaboration with V. K. Birman, J. E. Martin and E. Meiburg. We thank Yi-Jiun Lin for helpful comments on an earlier draft of this paper. This work was supported by the National Science Foundation under Grant CTS-0209194.

REFERENCES

- BAINES, P. G. 1995 *Topographic Effects in Stratified Flows*. Cambridge University Press.
- BAINES, W. D., ROTTMAN, J. W. & SIMPSON, J. E. 1985 The motion of constant-volume air cavities released in long horizontal tubes. *J. Fluid Mech.* **161**, 313–327.
- BARR, D. I. H. 1967 Densimetric exchange flows in rectangular channels. *Houille Blanche* **22**, 619–631.
- BENJAMIN, T. B. 1968 Gravity currents and related phenomena. *J. Fluid Mech.* **31**, 209–248.
- BIRMAN, V., MARTIN, J. E. & MEIBURG, E. 2005 The non-Boussinesq lock-exchange problem. Part 2. High-resolution simulations. *J. Fluid Mech.* **537**, 125–144.
- CHU, V. H. & BADDOUR, R. E. 1977 Surges, waves and mixing in two-layer density stratified flow. *Proc. 17th Congr. Intl. Assocn Hydraul. Res.* vol. 1, 303–310.
- DALY, B. J. & PRACHT, W. E. 1968 Numerical study of density-current surges. *Phys. Fluids* **11**, 15–30.
- GARDNER, G. C. & CROW, I. G. 1970 The motion of large bubbles in horizontal channels. *J. Fluid Mech.* **43**, 247–255.
- GRÖBELBAUER, H. P., FANNELØP, T. K. & BRITTER, R. E. 1993 The propagation of intrusion fronts of high density ratios. *J. Fluid Mech.* **250**, 669–687.
- HÄRTEL, C., MEIBURG, E. & NECKER, F. 2000 Analysis and direct numerical simulation of the flow at a gravity current head. Part 1. Flow topology and front speed for slip and no-slip boundaries. *J. Fluid Mech.* **418**, 189–212.
- HUPPERT, H. E. & SIMPSON, J. E. 1980 The slumping of gravity currents. *J. Fluid Mech.* **99**, 785–799.
- KELLER, J. J. & CHYOU, Y.-P. 1991 On the hydraulic lock exchange problem. *J. Appl. Math. Phys.* **42**, 874–909.
- KEULEGAN, G. H. 1958 The motion of saline fronts in still water. *Natl Bur. Stand. Rep.* 5813.
- KLEMP, J. B., ROTUNNO, R. & SKAMAROCK, W. C. 1994 On the dynamics of gravity currents in a channel. *J. Fluid Mech.* **269**, 169–198.
- KLEMP, J. B., ROTUNNO, R. & SKAMAROCK, W. C. 1997 On the propagation of internal bores. *J. Fluid Mech.* **331**, 81–106.
- LANE-SERFF, G. F., BEAL, L. M. & HADFIELD, T. D. 1995 Gravity current flow over obstacles. *J. Fluid Mech.* **292**, 39–53.

- LANE-SERFF, G. F. & WOODWARD, M. D. 2001 Internal bores in two-layer exchange flows over sills. *Deep-Sea Res. I* **48**, 63–78.
- ROTTMAN, J. W. & LINDEN, P. F. 2001 Gravity currents. In *Stratified Flows in the Environment* (ed. R. H. J. Grimshaw), pp. 87–117. Kluwer.
- ROTTMAN, J. W. & SIMPSON, J. E. 1983 Gravity currents produced by instantaneous releases of a heavy fluid in a rectangular channel. *J. Fluid Mech.* **135**, 95–110.
- SHIN, J. O., DALZIEL, S. B. & LINDEN, P. F. 2004 Gravity currents produced by lock exchange. *J. Fluid Mech.* **521**, 1–34.
- SIMPSON, J. E. & BRITTER, R. E. 1979 The dynamics of the head of a gravity current advancing over a horizontal surface. *J. Fluid Mech.* **94**, 477–495.
- WILKINSON, D. L. 1982 Motion of air cavities in long horizontal ducts. *J. Fluid Mech.* **118**, 109–122.
- WOOD, I. R. & SIMPSON, J. E. 1984 Jumps in layered miscible fluids. *J. Fluid Mech.* **140**, 329–342.
- YIH, C. S. 1965 *Dynamics of Nonhomogeneous Fluids*. Macmillan.
- YIH, C. S. & GUHA, C. R. 1955 Hydraulic jump in a fluid system of two layers. *Tellus* **7**, 358–366.